CHEMISTRY OF MATERIALS

pubs.acs.org/cm

Article

Epitaxial Thin-Film Spinel Oxides as Oxygen Reduction Electrocatalysts in Alkaline Media

Yao Yang,[▽] Rui Zeng,[▽] Hanjong Paik,[▽] Ding-Yuan Kuo, Darrell G. Schlom, Francis J. DiSalvo, David A. Muller, Jin Suntivich, and Héctor D. Abruña*

Cite This: *Chem. Mater.* 2021, 33, 4006−4013

Read Online

ACCESS | Metrics & More | Article Recommendations | Supporting Information

ABSTRACT: Designing nonprecious electrocatalysts for the challenging oxygen reduction reaction (ORR) is of paramount importance to advance hydrogen fuel cell technologies. Elucidating the ORR mechanism requires well-controlled surface structures and compositions at the atomic scale, which are often lacking in nanoparticle studies. Here, we report the growth and ORR activity in alkaline media of (100)-oriented, crystalline spinel oxide thin films prepared with atomic layer precision by molecular beam epitaxy. Co active sites were incorporated into a more conductive Fe_3O_4 host to mitigate the insulating nature of Co_3O_4. Co-doped Fe_3O_4, with Co-doping levels from 0 to 25%, were grown epitaxially on single-crystal MgO (100) substrates, prepared as thin-film electrodes with a front contact, and tested in a customized rotating disk electrode (RDE) assembly. The reliability of this RDE assembly for quantitative ORR activity measurements was validated with both polycrystalline Pd thin films and conductive RuO_2 (110) on an insulating substrate. Co-doped Fe_3O_4, with a 15% Co-doping level, achieved the optimal ORR activity in alkaline media. This was ascribed to the maximum number of Co active sites that could be incorporated without affecting the conductivity of the Fe_3O_4 matrix. This study enables investigating the ORR processes in a new realm—on epitaxial thin-film spinel oxides customized with a precision previously reserved/achieved for the semiconductor industry—and provides new strategies to overcome the generally low conductivity of metal oxide films as electrocatalysts in alkaline fuel cells.

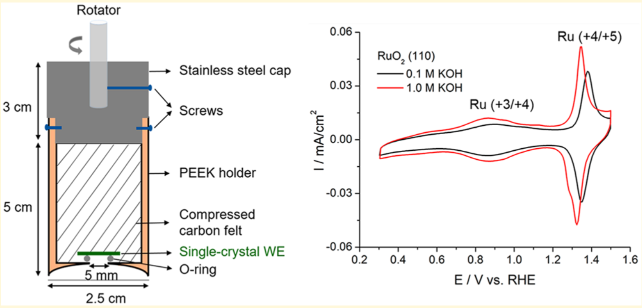

INTRODUCTION

Hydrogen fuel cells serve as high-efficiency energy conversion devices for converting hydrogen directly into electricity. This technology, when combined with water electrolysis, can balance the mismatch between intermittent solar/wind energy and the need for continuous power in existing electrical grids.[1,2] During the past two decades, hydrogen fuel cells, especially proton exchange membrane fuel cells (PEMFCs), have witnessed tremendous progress in both electrocatalysts and membrane technologies.[2−4] The high energy efficiency (>65%) and volumetric/gravimetric power density of PEMFCs have enabled a steadily growing market for fuel cell electric vehicles (FCEVs).[2] Unfortunately, PEMFCs still inherently require a large amount of expensive platinum group metal (PGM) based electrocatalysts to catalyze the sluggish oxygen reduction reaction (ORR).[5−8] The cost of such electrocatalysts is projected to be the largest single component (∼40%) of a PEMFC stack.[9] Recently, alkaline/anion exchange membrane fuel cells (AEMFCs) have emerged as an alternative technology[10,11] since they enable the use of nonprecious metal electrocatalysts, such as metal-N-doped carbons,[12,13] perovskites,[14,15] and, particularly, 3d transition metal oxides,[16−23] due to their low cost and high performance. We recently developed a novel family of 15 AB_2O_4 spinel oxides (A = Mn, Fe, Co, Ni, Cu; B= Mn, Fe, Co) as ORR electrocatalysts for alkaline fuel cells.[24] Among those, Mn−Co spinel oxides exhibited significantly enhanced ORR activities relative to both Co_3O_4/C and Mn_3O_4/C and rivalled Pt/C electrocatalysts in alkaline fuel cells.[25] The superior performance of these Co−Mn spinels was ascribed to the synergistic effect of Co and Mn, as evidenced by *operando* X-ray absorption spectroscopy measurements.[26,27] Furthermore, Mn−Co−Fe trimetallic oxides exhibited enhanced long-term durability, which was ascribed to the Fe maintaining the structural integrity while Co and Mn served as coactive catalytic sites.[28]

While there have been numerous studies on metal oxide electrocatalysts, mechanistic studies on well-defined surfaces have been elusive. Despite tremendous efforts in developing alkaline ORR electrocatalysts, it is a formidable task to

Received: February 2, 2021
Revised: May 7, 2021
Published: May 24, 2021

https://doi.org/10.1021/acs.chemmater.1c00388

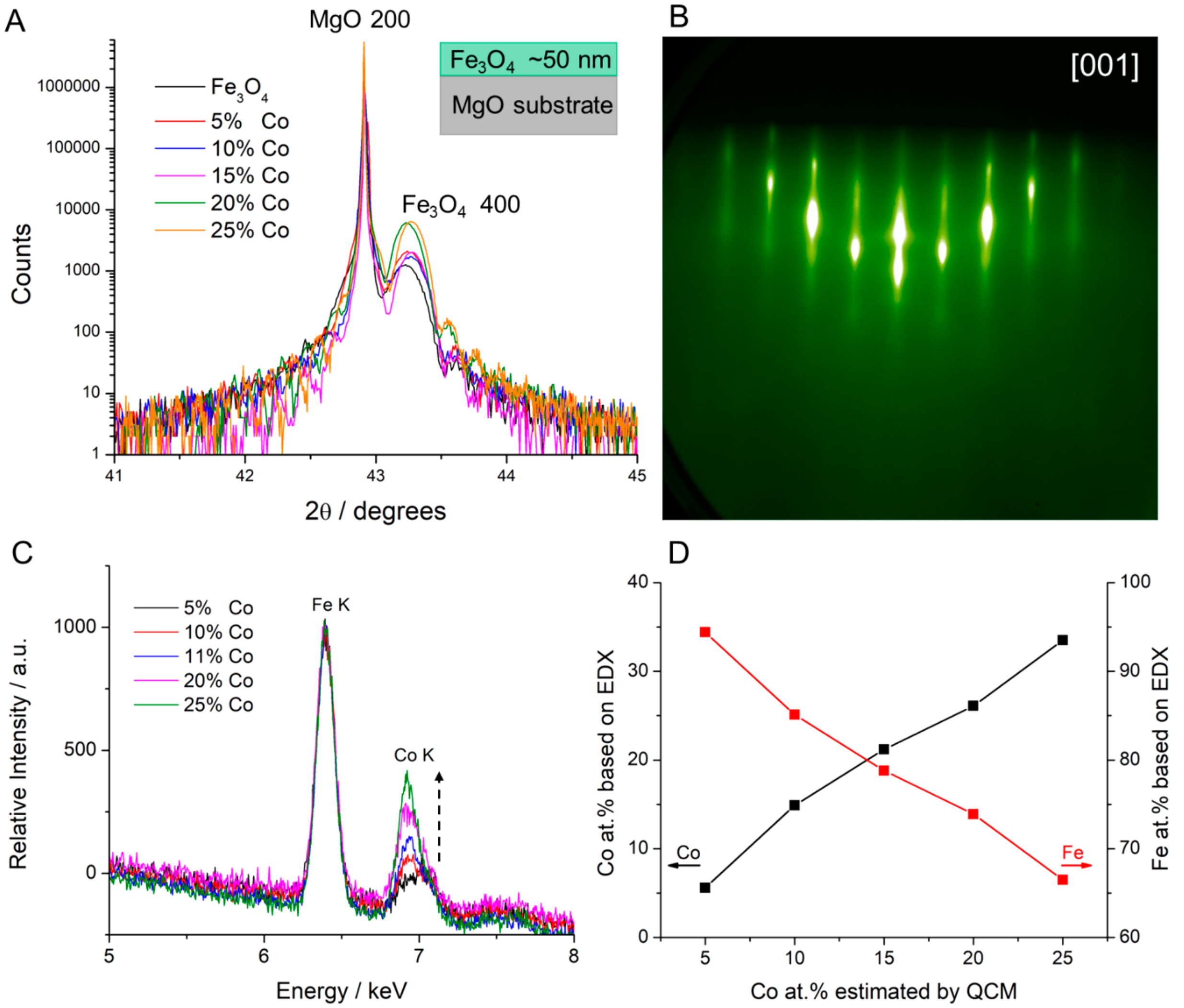

Figure 1. Structural characterization of Co-doped Fe_3O_4. (A) X-ray diffraction (XRD) patterns (θ–2θ scan) of a series of epitaxial Co-doped Fe_3O_4 films grown on single-crystal MgO (100) substrates by molecular beam epitaxy (MBE). (B) Reflection high-energy electron diffraction (RHEED) pattern of 15% Co-doped Fe_3O_4 at the end of an ~50 nm thick layer with the beam along the [001] direction. (C) SEM-EDX spectra of a series of Co-doped Fe_3O_4 films at 30 keV. The dashed arrow shows increasingly stronger Co K-edges after all the spectra were normalized to the Fe K-edges. (D) Quantitative analysis of the relative Co and Fe atom % as a function of nominal Co atom % estimated by a quartz crystal microbalance (QCM) in the MBE chamber.

simultaneously control surface morphology, atomic arrangement, particle size and its distribution, and crystal structures of metal oxide nanoparticles. Those factors often convolute and complicate our understanding of the structure–activity relationships. Single crystals, especially Pt and Au prepared by the flame annealing technique (Clavilier method),[29] have profoundly shaped the atomic and molecular-level understanding of electrochemical reaction mechanisms. Thus, we are interested in preparing metal oxides of similar quality. Herein, we report our investigation of metal-oxide thin films with a well-defined surface structure to better understand the structure-(re)activity relationship(s) and identify the active site(s) and reaction path(s) for the ORR in alkaline media. Thin-film electrocatalysts have been prepared using magnetron sputtering,[30−32] chemical vapor deposition,[33] inkjet printing,[34] etc., which often result in polycrystalline films with a significant surface roughness and defect density. In this work, epitaxial thin-film metal oxides were prepared on single-crystal substrates by molecular beam epitaxy (MBE) layer-by-layer growth. MBE enables the growth of high-quality metal oxide films with well-defined, atomically flat surfaces and minimal defects, which can overcome the aforementioned challenges associated with nanoparticles and polycrystalline thin films.[35] Procedures for characterizing and preparing thin-film electrodes with a front contact are described in detail. A customized thin-film rotating disk electrode (RDE) assembly was designed to reliably and rigorously characterize the electrochemical behavior of these thin-film electrodes.[36] Although epitaxial thin-film metal oxides have a well-defined structure and composition with minimal defects, relative to nanoparticle counterparts, spinel oxides, such as Co_3O_4 or Mn_3O_4 grown by MBE, are wide-band gap materials with too low conductivity (MΩ-level resistance) to serve as working electrodes. Spinel oxide nanoparticles largely bypass such problems by having small particle sizes embedded in a conductive carbon matrix and with defects and/or oxygen vacancies, which can serve as charge transfer paths.[24,25] In order to tackle this challenge, we incorporated a small amount of Co active sites into a more conductive Fe_3O_4 matrix. The Co-doped Fe_3O_4 showed improved ORR activity, relative to pure Fe_3O_4. Other strategies, such as annealing Co_3O_4 to create oxygen

https://doi.org/10.1021/acs.chemmater.1c00388
Chem. Mater. 2021, 33, 4006−4013

vacancies or growing an ultrathin (few nanometers thick) Co_3O_4 film on Fe_3O_4, are also discussed as ways to mitigate the conductivity issues of Co_3O_4 thin films.

■ RESULTS AND DISCUSSION

Fe_3O_4 and Co-doped Fe_3O_4 epitaxial thin films were grown on MgO (100) substrates by MBE. Co-doped Fe_3O_4 films were prepared by exposing the MgO substrate (heated at 350 °C) to thermally evaporated Co and Fe atomic beams in a pure O_2 environment. The lattice mismatch between (100)-oriented Fe_3O_4 and (100)-oriented MgO is only 0.5% (a_{Fe3O4} = 8.394 Å differs by 0.5% from twice a_{MgO} = 4.217 Å), which promotes the epitaxial growth of Fe_3O_4 on the MgO (100) substrate. A θ–2θ X-ray diffraction scan of Co-doped Fe_3O_4 shows the characteristic diffraction peaks of MgO 200 and the nearby Fe_3O_4 400 (Figure 1A), which corroborate the spinel crystal structure of the epitaxially grown Co-doped Fe_3O_4. XRD over a wide 2θ range shows a single-phase Co-doped Fe_3O_4 solid solution with no impurity of Co oxides (Figure S1). The 2θ angles of Co-doped Fe_3O_4 at different Co doping levels are 43.24 ± 0.02° with a minimal shift, which is consistent with the negligible difference between the 400 peaks of bulk Fe_3O_4 and $CoFe_2O_4$ (i.e., 33% Co) standards (Figure S2). X-ray reflectivity (XRR) measurements of a 45 nm thick Fe_3O_4 film show clear thickness oscillations (Figure S3), consistent with the growth of a smooth film. Reflection high-energy electron diffraction (RHEED) of a 15% Co-doped Fe_3O_4 film shows a sharp and streaky pattern, and the elongated bright spots are the intersections of the reciprocal rods with the Ewald sphere (Figure 1B).[37] Such a RHEED patten indicates a high-quality epitaxial thin film with a smooth surface. The RHEED patterns of other Co-doped Fe_3O_4 films were similar (Figure S4).

The surface morphology and elemental compositions of Co-doped Fe_3O_4 were characterized by scanning electron microscopy (SEM) and energy dispersive X-ray (EDX) spectroscopy, respectively. An electron beam at 30 keV can penetrate the 50 nm thick Co-doped Fe_3O_4 films and thus yield an average composition. As shown in Figure 1C, EDX spectra of Co-doped Fe_3O_4 films, normalized to Fe K-edges, exhibit a gradually increasing Co K-edge intensity suggesting a relatively higher Co content, as indicated by the dashed arrow in the figure. EDX quantification in Figure 1D indicated that the relative contents of Co atom %, based on EDX analysis, were consistent with the values estimated from the quartz crystal microbalance (QCM). Given that the QCM calibration often has a relative error of about 10%, EDX quantification confirmed the successful synthesis of Co-doped Fe_3O_4 films with well-controlled compositions.

MBE-grown metal oxide thin films were prepared as electrodes with a front electrical contact for electrochemical measurements. As shown in Figure 2A, all four edges of a 1 × 1 cm^2 thin film were gently scratched and covered with a Ga–In eutectic. The sides and corners of the thin films were coated with Ag paint to provide good contact to circumvent the insulating nature of the oxide substrate. A Teflon O-ring defined a round region (diameter = 5 mm) as the exposed electrode area (0.196 cm^2) and prevented electrolyte from contacting the Ga–In or Ag paint. This is especially important for Ag since it is an active catalyst for the ORR in alkaline media. In order to perform standard electrochemical measurements, a custom-built rotating disk electrode (RDE) holder assembly was designed and made of polyether ether ketone (PEEK) (Figure 2B). As a hydrophilic material, PEEK can effectively prevent gas bubbles from forming on the electrode surface. It is also much harder, relative to hydrophobic and soft polytetrafluoroethylene (PTFE) Teflon. A thin-film electrode, together with an O-ring, were placed against the thin wall at the bottom of the PEEK holder. The RDE holder was then filled with a carbon felt and compressed tightly with a stainless steel cap. Three screws helped fix the position of the cap and connected the RDE holder to a commercial rotator (Pine Instruments). It is critical to ensure that there is no leakage of electrolyte passing through the O-ring since multiple components can contribute to a current much larger than that from the MBE-grown oxide electrode front surface. This includes the Ag paint, Pt coating on the back of the oxide substrate, and carbon felt. The shallow feature at the bottom of the RDE holder was designed to allow convective–diffusion processes similar to a flat RDE.[38]

To validate the feasibility and reliability of this customized RDE assembly, thin-film Pd, a well-known benchmark ORR catalyst in alkaline media,[30,39] was prepared employing the same procedure and loaded/assembled for RDE measurements (Figure 2C). The total resistance of the Pd film and the carbon felt was 2.5 Ω, close to that of a typical commercial RDE (2–5 Ω). RDE polarization profiles of the Pd thin-film electrode were recorded in O_2-saturated 1 M KOH at 5 mV/s and rotation rates from 100 to 1600 rpm. Well-defined current plateaus indicated that the Pd thin films were able to achieve a diffusion-limited response. The larger background noise at 1600 rpm is likely due to the turbulence/vortex formed by the mechanical instability (cavitation) of the RDE in solution and a less stable electrical connection between the rod and the carbon brush in the motor. The Levich plot in Figure 2D showed an excellent linear correlation between the diffusion-limited current density (I_d) and $\omega^{1/2}$ (rotation rate in rpm) with an R^2 value of 0.998. The electron transfer number, n, was calculated to be 4.0 ± 0.1 based on the Levich equation ($I_d = 0.62nFD^{2/3}\upsilon^{-1/6}\omega^{1/2}C_{O2}$ where n, F, D, υ and C_{O2} are the electron transfer number, Faraday's constant, diffusion coefficient, kinematic viscosity, and bulk concentration of O_2 in the electrolyte at 25 °C). The Pd film showed the characteristic current density of about 3.7 mA/cm^2 at 1600 rpm, a typical value corresponding to a $4e^-$ process. It should be noted that the I_d values for a $4e^-$ ORR process in 1 and 0.1 M KOH at 1600 rpm are 3.7 and 5.5 mA/cm^2, respectively, since the C_{O2} in 1 M KOH is 8.42×10^{-4} M, only 70% of that in 0.1 M KOH (1.21×10^{-2} M).[40] We used 1 M KOH in this work since it has a lower solution resistance than 0.1 M KOH and is a closer approximation of the high OH^- concentration in a membrane electrode assembly (MEA).

With the validation of the thin-film Pd catalysts, we further employed a (110)-oriented RuO_2 film grown on a TiO_2 (110) substrate to examine the application of the custom-built RDE for MBE-grown metal oxides. Since RuO_2 films are conductive, while the TiO_2 substrate is insulating, the success of the RDE measurements relied on the quality of the front contact. Electrochemical impedance spectroscopy (EIS) measurements showed a total ohmic resistance close to an equivalent measurement on platinum (~50 Ω), indicating a good electrical connection. As shown in Figure 2E, the ORR polarization profiles in the Ar and O_2 environments clearly showed that RuO_2 is active in catalyzing the reduction of oxygen. RuO_2 achieved a current density at 0.3 V of 0.32 mA/cm^2, a value much smaller than that of the Pd thin film (3.7 mA/cm^2), clearly indicating that RuO_2 is a poorer electrocatalyst when compared with Pd for the ORR in alkaline media. The CV profiles of RuO_2 showed the advantage of MBE-grown metal oxides (Figure 2F). Two

https://doi.org/10.1021/acs.chemmater.1c00388
Chem. Mater. 2021, 33, 4006−4013

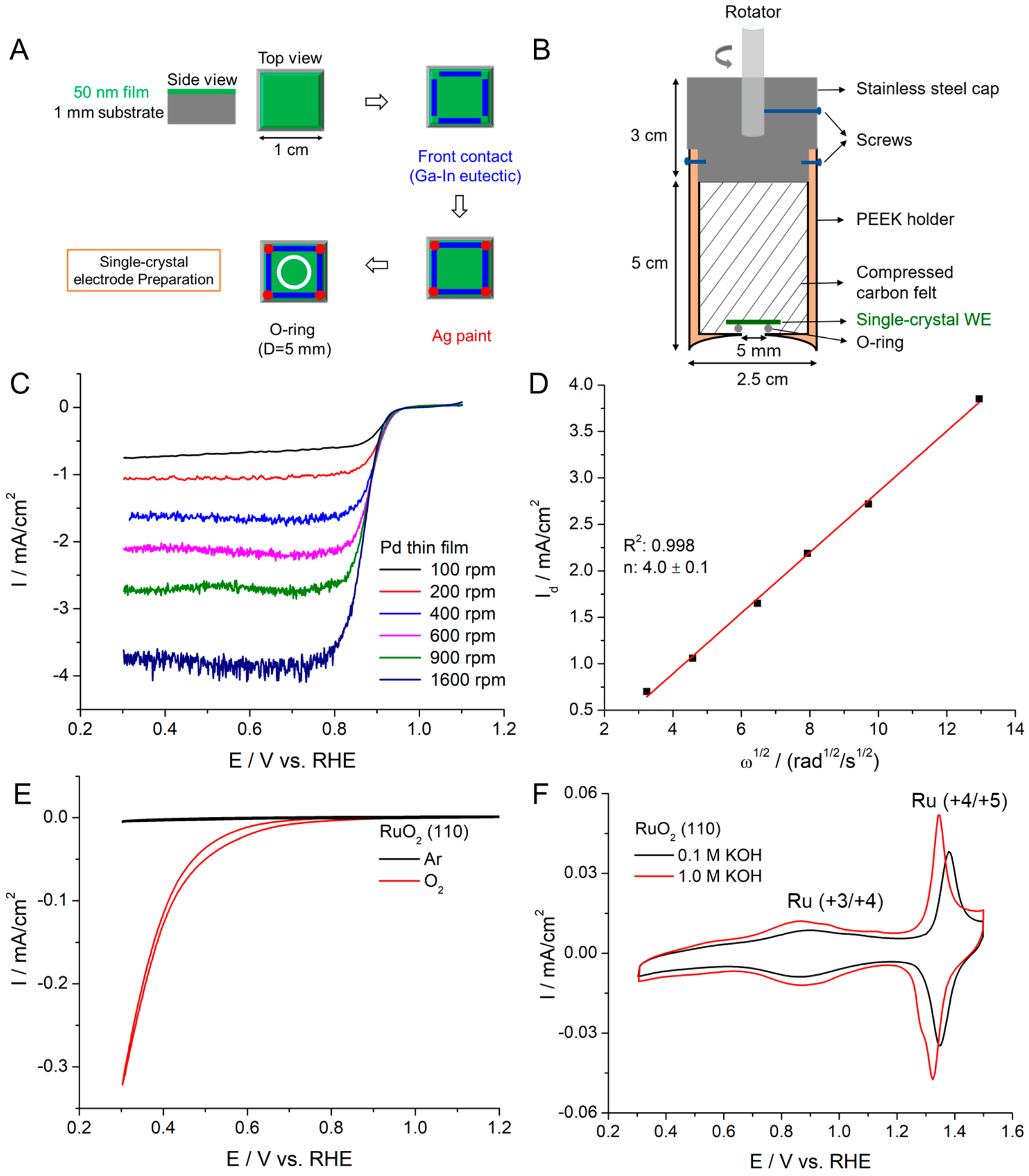

Figure 2. Methodology for thin-film rotating disk electrode (RDE) measurements. (A) Procedures for preparing epitaxial thin-film electrodes with a front face contact to circumvent the insulating nature of the metal oxide substrate. (B) Schematic of the customized RDE holder. Carbon felt is filled and compressed to make good electrical contact with the side and the front of the epitaxial thin-film working electrode (WE). (C, D) RDE measurements of a polycrystalline Pd film at 5 mV/s and various rotation rates in O_2-sat. 1 M KOH and the corresponding Koutecky−Levich plot showing a well-defined 4e$^-$ process. (E) RDE measurements of an epitaxial thin-film conductive RuO_2 on an insulating TiO_2 (110) substrate in both Ar and O_2-sat. 1 M KOH at 1600 rpm and 5 mV/s to validate the feasibility of RDE measurements of epitaxial thin-film metal oxides. (F) CV profiles of RuO_2(110) at 50 mV/s in Ar-sat. 0.1 and 1 M KOH showing two well-defined Ru redox couples belonging to the epitaxial thin-film RuO_2 (110).

reversible redox couples were clearly identified. We assigned these redox peaks to $Ru^{3+/4+}$ (OH adsorption) and $Ru^{4+/5+}$ (O adsorption).[41−44] Compared with 0.1 M KOH (Table S2), both redox couples shifted to less positive potentials in 1 M KOH, suggesting that OH and O tend to adsorb more easily on RuO_2 surfaces at a higher pH. Similar trends were also found in studies of MBE-grown IrO_2[45] and single-crystal Pt (Figure S4).[46] CV profiles of RuO_2 in 1 M KOH showed that the total charges corresponding to OH and O adsorption were 22% and 38% larger than in 0.1 M KOH, indicating a higher OH saturation coverage at higher pH (Table S1). The O adsorption peak of RuO_2 in 1 M KOH was calculated to have a smaller full-width at half-maximum (fwhm) of 48 mV, smaller than that in 0.1 M KOH (60 mV), suggesting a stronger attractive interaction

https://doi.org/10.1021/acs.chemmater.1c00388
Chem. Mater. 2021, 33, 4006−4013

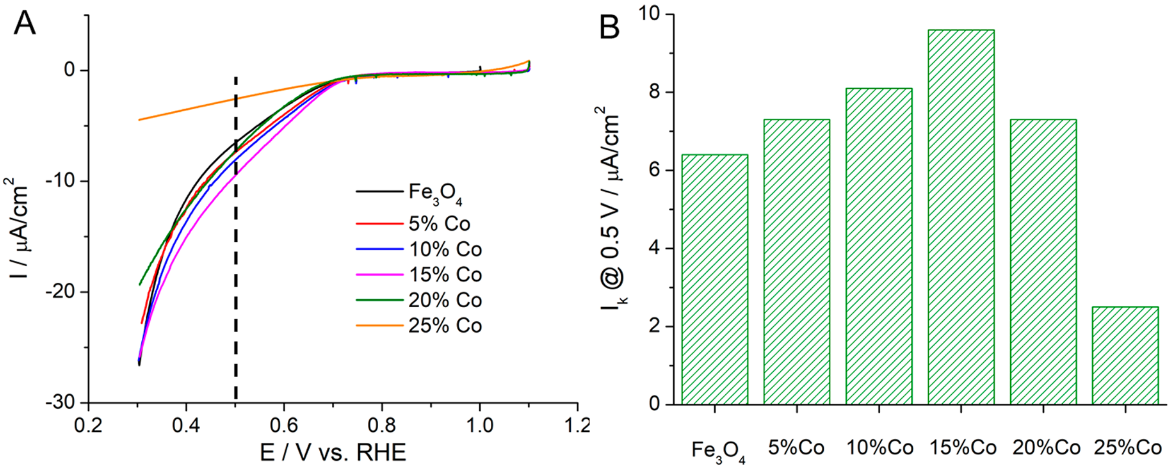

Figure 3. (A) RDE polarization profiles of various Co-doped Fe_3O_4 at 900 rpm and 5 mV/s in O_2-sat. 1 M KOH. (B) Kinetic current density, as an ORR activity metric, of Co-doped Fe_3O_4 at 0.5 V vs RHE, showing the optimal activity of 15% Co-doped Fe_3O_4.

among adsorbates at higher pH (Table S1).[46] The charge density of O adsorption in 1.0 M KOH was calculated to be around 60 μC/cm^2, which corresponds to about 3/4 coverage at coordinatively unsaturated sites (Table S1), a typical value for maximum coverage of surface oxides.[46] Such well-defined features can only be expected from high-quality single-crystal metal oxides and are much more pronounced when compared with early electrochemical studies of RuO_2 polycrystalline particles in alkaline media.[41] In summary, we have employed polycrystalline Pd films and MBE-grown RuO_2 (110) films as representative examples to establish the reliability of our RDE methodology for preparing and evaluating single-crystal metal oxide electrodes as thin-film RDEs.

The electrochemical activity of epitaxial thin films of Co-doped Fe_3O_4 were examined via RDE measurements (Figure 3), following the same procedure discussed above. The ORR polarization profiles in Figure 3A present the ORR activities of Co-doped Fe_3O_4 films with different Co-doping levels in 1 M KOH at 900 rpm and 5 mV/s. The ORR activities show a steady increase from 0 to 15% Co followed by a drastic decrease at 20 and 25% Co. The onset potentials for Co-doped Fe_3O_4 films were estimated to be around 0.7 V vs RHE, which are significantly lower than either Pd (~1.0 V) or RuO_2 (~0.9 V). Co-doped Fe_3O_4 achieved a current density of ~25 μA/cm^2 at 0.3 V, significantly lower than that of Pd and RuO_2. We believe that the low overall activity of Co-doped Fe_3O_4 is largely governed by the inactive Fe_3O_4 substrate. In order to quantitatively assess the ORR activities of Co-doped Fe_3O_4 films, and their kinetic current densities at 0.5 V vs RHE were determined and are plotted in Figure 3B, based on the Koutecky−Levich equation, assuming an I_d of 2.7 mA/cm^2 at 900 rpm based on the study of the Pd thin films (Figure 2C). Among the family of Co-doped Fe_3O_4 films studied, the electrode with a 15% Co-doping level achieved a maximal I_k of 9.6 μA/cm^2, 50% higher than that of pure Fe_3O_4 (6.4 μA/cm^2). Further increases in the Co-doping levels led to a dramatic decrease in activity. CV profiles of Co-doped Fe_3O_4 films showed larger oxidation currents when the Co atom % increased from 0 to 15% Co but a significantly smaller current at 25% (Figure S6). Electrochemical impedance spectroscopy (EIS) measurements indicated that Co-doped Fe_3O_4 films with 0−15% Co had a reasonably low ohmic resistance of about 1 kΩ or lower, while Co-doped Fe_3O_4 films with 25% Co had a resistance of 300 kΩ (Table S2). Since our Co-doped Fe_3O_4 films showed μA-level currents, *iR*-correction with 1 kΩ would have a negligible impact on the voltage compensation. Thus, we can ascribe the increase in the activity from 0 to 15% Co-doping levels to the increasing Co active sites with minimal impact from the *iR* drop. The same thing, however, cannot be said for 25% Co. We ascribe the large activity decrease at 25% to the significantly higher resistance, which is also evident from the nearly capacitive behavior of the CV profile (gray line in Figure S6). In fact, further increasing the Co-doping levels to 30% led to an ohmic resistance larger than 10 MΩ, which is much too resistive for any meaningful electrochemical measurements.

The aforementioned strategy to incorporate Co active sites into a more conductive Fe_3O_4 lattice provides a pathway to tackle the low conductivity issue of Co_3O_4, albeit with the limitation of how much Fe can be substituted by Co. Other strategies, such as creating oxygen vacancies by annealing treatments, are discussed below. Co_3O_4 thin films were epitaxially grown on $MgAl_2O_4$. $MgAl_2O_4$ was chosen as the substrate because of its close lattice match of 0.1%; the crystal structure was characterized by XRD (Figure S7). The as-grown Co_3O_4 films had an ohmic resistance of over 10 MΩ and thus showed a nearly pure capacitive behavior with a nA-level current in the CV profiles (Figure S8), which explained why high Co-doping levels in Fe_3O_4 (≥30%) eventually lead to insulating films. In an attempt to create oxygen vacancies so as to increase conductivity, Co_3O_4 films were annealed in an Ar atmosphere from 200 to 900 °C for up to 24 h. Unfortunately, negligible changes in the ohmic resistance were observed after the annealing treatment in Ar, suggesting that no oxygen vacancies were formed. We therefore subjected the Co_3O_4 films to a more reducing environment of forming gas (5% H_2 and 95% N_2). Annealing temperatures were carefully ramped up from 200 to 300 °C while monitoring changes in the ohmic resistance. At an annealing temperature of 250 °C, the ohmic resistance dropped significantly from 90 kΩ to only 70 Ω (Table S3). XRD of Co_3O_4 after annealing in the forming gas at 250 °C showed evidence of metallic Co formed from Co_3O_4 films on $MgAl_2O_4$ (Figure S9). Electrochemical measurements of Co_3O_4 after annealing in forming gas at 250 °C exhibited unstable redox reactions among Co(0), Co(+2), and Co(+3) and evidence of Co dissolution after 20 CV cycles (Figure S10). Electrochemical measurements of Co_3O_4 annealed at 200 and 225 °C in forming gas did not yield reliable electrochemical data given their MΩ-level resistance. Another strategy would be to grow a thin (few atomic-layer thick) Co_3O_4 layer on top of a Fe_3O_4 epitaxial film or substrate to provide enough active sites while maintaining a low bulk resistance. Unfortunately, Co_3O_4 (a = 8.072 Å) and Fe_3O_4 (a = 8.394 Å) have a large lattice mismatch of 3.8%, which makes high-quality epitaxial MBE growth very challenging. Additionally, Co tends to form the Co_3O_4 phase in 10% O_3 and CoO in pure O_2, while Fe forms Fe_2O_3 in 10% O_3 and Fe_3O_4 in pure O_2. Such incompatibility in growth conditions makes the growth of layered Co_3O_4/Fe_3O_4 structures practically inaccessible.

CONCLUSIONS

In summary, we have prepared well-defined Co-doped Fe_3O_4 films to controllably introduce Co active sites. By embedding Co into a conductive Fe_3O_4 substrate, we were able to significantly mitigate the insulating nature of Co_3O_4 which allowed us to test the ORR electrocatalysis on Co atoms in the spinel structure. Quantitative ORR activity measurements were achieved in a custom-built RDE. The 15% Co-doped Fe_3O_4 exhibited enhanced/optimized ORR activity, relative to pure Fe_3O_4. Other strategies to improve the conductivity of Co_3O_4 were also pursued, such as a postannealing treatment to create oxygen vacancies and the use of a thin Co_3O_4 on Fe_3O_4 layered epitaxial heterostructure. This study demonstrates the need to increase the conductivity of single-crystal thin-film 3d metal oxides in order to allow catalytically active sites to participate in electrocatalysis. We anticipate that advances in other single-crystal metal oxide films will result in a deeper mechanistic understanding of nonprecious metal and metal oxide electrocatalysts for the ORR, which is the cornerstone for the implementation of hydrogen fuel cell technologies.

EXPERIMENTAL SECTION

Molecular-Beam Epitaxy (MBE) Growth. Fe_3O_4 and Co-doped Fe_3O_4 films were epitaxially grown on single-crystal MgO (100) in a pure O_2 environment at a background pressure of 1×10^{-6} Torr using the PARADIM thin-film growth facility at Cornell University. The fluxes of the Fe and Co molecular beams were calibrated using a quartz crystal microbalance (QCM). With the Fe source set to a temperature of 1150 °C, the Fe flux was about 2.5×10^{13} atom/(cm^2·s). The doping levels of Co (0−25 atom %) were controlled by adjusting the temperature of the Co source from 1150 to 1280 °C to tune the Co flux to achieve the desired Co/Fe atomic ratio. The temperature of the MgO substrate was set at 350 °C. Similarly, Co_3O_4 films were grown on (100) and (111)-oriented single-crystal $MgAl_2O_4$ substrates in a background pressure of 1×10^{-6} Torr of 10% O_3. Ozone was used because in a pure O_2 environment at these growth conditions CoO forms. RuO_2 films were grown on single-crystal TiO_2 (110) using a distilled ozone oxidant (∼80% O_3) at a background pressure of 1×10^{-6} Torr since it is difficult to oxidize Ru. The film growth was monitored *in situ* during growth by reflection high-energy electron diffraction (RHEED).

Structural Characterization. As-grown epitaxial thin films were characterized by XRD (Rigaku Smartlab) using Cu Kα_1 radiation. All XRD patterns of Co-doped Fe_3O_4 were calibrated based on the precise position of the MgO 200 substrate peak ($2\theta = 42.91°$). The elemental composition was examined by scanning electron microscopy (SEM) and energy dispersive spectroscopy (EDX) (LEO 1550 FESEM) at Cornell CCMR facilities.

Electrochemical Measurements. MBE-grown metal oxide films were fabricated as electrodes following the procedure in Figure 2A. The Ga−In eutectic (Sigma-Aldrich) and Ag paint were used to make front contacts. Thin-film metal oxides (1×1 cm^2 $L \times W$, 1 mm H) served as working electrodes (WEs) and were loaded/mounted into a customized rotating disk electrode (RDE) assembly as shown in Figure 2B. Pd thin films (0.1 mm, AlfaAesar, 99.95%) were flame annealed before use. Teflon O-rings were cleaned with H_2O and ethanol to remove possible contamination when exposed to KOH solution. The 1.0 M KOH solution was freshly prepared with ultrapure H_2O (18.2 MΩ). Ag/AgCl in saturated KCl solution served as the reference electrode (RE) and a large-surface-area graphite rod was used as the counter electrode (CE). The potential difference between Ag/AgCl in saturated KCl and a reversible hydrogen electrode (RHE) in 1.0 M KOH was calculated to be 1.0258 V based on the Nernst equation. ORR measurements were carried on in oxygen-saturated 1 M KOH solution at room temperature (23 °C). Cyclic voltammetry (CV) measurements were performed in Ar-sat. 1.0 M KOH from 0.2 to 1.3 V at 20 mV/s for 10 cycles. ORR polarization profiles were obtained at 5 mV/s from 0.3 to 1.1 V vs RHE after CV cycles. The rotation rates were controlled to be from 0 to 1600 rpm to study the reaction kinetics. Electrochemical impedance spectroscopy (EIS) measurements were carried out with a Solartron potentiostat from 20 000 to 0.1 Hz.

ASSOCIATED CONTENT

Supporting Information

The Supporting Information is available free of charge at https://pubs.acs.org/doi/10.1021/acs.chemmater.1c00388.

> XRD, XRR, RHEED, and CV data, quantitative analysis of the adsorption peaks in the CV profiles, and ohmic resistances (PDF)

AUTHOR INFORMATION

Corresponding Author

Héctor D. Abruña − *Department of Chemistry and Chemical Biology, Cornell University, Ithaca, New York 14853, United States*; orcid.org/0000-0002-3948-356X; Email: hda1@cornell.edu

Authors

Yao Yang − *Department of Chemistry and Chemical Biology, Cornell University, Ithaca, New York 14853, United States*; orcid.org/0000-0003-0321-3792

Rui Zeng − *Department of Chemistry and Chemical Biology, Cornell University, Ithaca, New York 14853, United States*; orcid.org/0000-0002-7577-767X

Hanjong Paik − *Department of Materials Science and Engineering and Platform for the Accelerated Realization, Analysis, and Discovery of Interface Materials (PARADIM), Cornell University, Ithaca, New York 14853, United States*

Ding-Yuan Kuo − *Department of Materials Science and Engineering, Cornell University, Ithaca, New York 14853, United States*

Darrell G. Schlom − *Department of Materials Science and Engineering and Kavli Institute at Cornell for Nanoscale Science, Cornell University, Ithaca, New York 14853, United States; Leibniz-Institut für Kristallzüchtung, 12489 Berlin, Germany*; orcid.org/0000-0003-2493-6113

Francis J. DiSalvo − *Department of Chemistry and Chemical Biology, Cornell University, Ithaca, New York 14853, United States*

David A. Muller − *School of Applied and Engineering Physics and Kavli Institute at Cornell for Nanoscale Science, Cornell University, Ithaca, New York 14853, United States*; orcid.org/0000-0003-4129-0473

Jin Suntivich − *Department of Materials Science and Engineering and Kavli Institute at Cornell for Nanoscale Science, Cornell University, Ithaca, New York 14853, United States*; orcid.org/0000-0002-3427-4363

Complete contact information is available at:
https://pubs.acs.org/10.1021/acs.chemmater.1c00388

Author Contributions

$^{\nabla}$Y.Y., R.Z., and H.P. contributed equally to this work.

Notes

The authors declare no competing financial interest.

■ ACKNOWLEDGMENTS

This work was primarily supported by the Center for Alkaline-Based Energy Solutions (CABES), an Energy Frontier Research Center (EFRC) program supported by the U.S. Department of Energy, under Grant DE-SC0019445. This work made use of the SEM facility at the Cornell Center for Materials Research (CCMR), which is supported through the National Science Foundation Materials Research Science and Engineering Center (NSF MRSEC) program (DMR-1719875). The thin-film materials are based upon work supported by the National Science Foundation (Platform for the Accelerated Realization, Analysis, and Discovery of Interface Materials (PARADIM)) under Cooperative Agreement No. DMR-1539918.

■ REFERENCES

(1) Pivovar, B. Catalysts for Fuel Cell Transportation and Hydrogen Related Uses. *Nat. Catal.* **2019**, *2*, 562−565.

(2) Ayers, K. E.; Dalton, L. T.; Anderson, E. B. Efficient Generation of High Energy Density Fuel from Water. *ECS Trans.* **2012**, *41*, 27−38.

(3) Debe, M. Electrocatalyst Approaches and Challenges for Automotive Fuel Cells. *Nature* **2012**, *486*, 43−51.

(4) Gasteiger, H. A.; Kocha, S. S.; Sompalli, B.; Wagner, F. T. Activity Benchmarks and Requirements for Pt, Pt-alloy, and non-Pt Oxygen Reduction Catalysts for PEMFCs. *Appl. Catal., B* **2005**, *56*, 9−35.

(5) Kongkanand, A.; Mathias, M. F. The Priority and Challenge of High-Power Performance of Low-Platinum Proton-Exchange Membrane Fuel Cells. *J. Phys. Chem. Lett.* **2016**, *7*, 1127−1137.

(6) Xiong, Y.; Yang, Y.; Joress, H.; Padgett, E.; Gupta, U.; Yarlagadda, V.; Agyeman-Budu, D. N.; Huang, X.; Moylan, T. E.; Zeng, R.; Kongkanand, A.; Escobedo, F. A.; Brock, J. D.; DiSalvo, F. J.; Muller, D. A.; Abruña, H. D. Revealing the Atomic Ordering of Binary Intermetallics Using in Situ Heating Techniques at Multilength Scales. *Proc. Natl. Acad. Sci. U. S. A.* **2019**, *116*, 1974−1983.

(7) Xiong, Y.; Yang, Y.; DiSalvo, F. J.; Abruña, H. D. Pt-Decorated Composition-Tunable Pd-Fe@Pd/C Core-Shell Nanoparticles with Enhanced Electrocatalytic Activity toward the Oxygen Reduction Reaction. *J. Am. Chem. Soc.* **2018**, *140*, 7248−7255.

(8) Xiong, Y.; Yang, Y.; DiSalvo, F. J.; Abruña, H. D. Pt-Decorated Composition-Tunable Pd-Fe@Pd/C Core-Shell Nanoparticles with Enhanced Electrocatalytic Activity toward the Oxygen Reduction Reaction. *J. Am. Chem. Soc.* **2018**, *140*, 7248−7255.

(9) Papageorgopoulos, D. *2019 Annual Merit Review and Peer Evaluation Meeting in Fuel Cells Program Area*; U.S. Department of Energy: Washington, DC.

(10) Lu, S.; Pan, J.; Huang, A.; Zhuang, L.; Lu, J. Alkaline Polymer Electrolyte Fuel Cells Completely Free from Noble Metal Catalysts. *Proc. Natl. Acad. Sci. U. S. A.* **2008**, *105*, 20611−20614.

(11) Wang, Y.; Yang, Y.; Jia, S.; Wang, X.; Lyu, K.; Peng, Y.; Zheng, H.; Wei, X.; Ren, H.; Xiao, L.; Wang, J.; Muller, D. A.; Abruña, H. D.; Hwang, B. J.; Lu, J.; Zhuang, L. Synergistic Mn-Co Catalyst Outperforms Pt on High-Rate Oxygen Reduction Reaction for Alkaline Polymer Electrolyte Fuel Cells. *Nat. Commun.* **2019**, *10*, 1506.

(12) Chung, H. T.; Cullen, D. A.; Higgins, D.; Sneed, B. T.; Holby, E. F.; More, K. L.; Zelenay, P. Direct Atomic-Level Insight into the Active Sites of a High-Performance PGM-Free ORR Catalyst. *Science* **2017**, *357*, 479−484.

(13) Ren, H.; Wang, Y.; Yang, Y.; Tang, X.; Peng, Y.; Peng, H.; Xiao, L.; Lu, J.; Abruña, H. D.; Zhuang, L. Fe/N/C Nanotubes with Atomic Fe Sites: A Highly Active Cathode Catalyst for Alkaline Polymer Electrolyte Fuel Cells. *ACS Catal.* **2017**, *7*, 6485−6492.

(14) Suntivich, J.; Gasteiger, H. A.; Yabuuchi, N.; Nakanishi, H.; Goodenough, J.; Shao-Horn, Y. Design Principles for Oxygen-Reduction Activity on Perovskite Oxide Catalysts for Fuel Cells and Metal-Air Batteries. *Nat. Chem.* **2011**, *3*, 647−647.

(15) Xu, X.; Wang, W.; Zhou, W.; Shao, Z. Recent Advances in Novel Nanostructuring Methods of Perovskite Electrocatalysts for Energy-Related Applications. *Small* **2018**, *2*, 1800071.

(16) Liang, Y.; Li, Y.; Wang, H.; Zhou, J.; Wang, J.; Regier, T.; Dai, H. Co_3O_4 Nanocrystals on Graphene as a Synergistic Catalyst for Oxygen Reduction Reaction. *Nat. Mater.* **2011**, *10*, 780−786.

(17) Xiong, Y.; Yang, Y.; DiSalvo, F. J.; Abruña, H. D. Metal-Organic-Framework-Derived Co-Fe Bimetallic Oxygen Reduction Electrocatalyst for Alkaline Fuel Cells. *J. Am. Chem. Soc.* **2019**, *141*, 10744−10750.

(18) Li, C.; Han, X.; Cheng, F.; Hu, Y.; Chen, C.; Chen, J. Phase and Composition Controllable Synthesis of Cobalt Manganese Spinel Nanoparticles towards Efficient Oxygen Electrocatalysis. *Nat. Commun.* **2015**, *6*, 7345.

(19) Yang, Y.; Zeng, R.; Xiong, Y.; DiSalvo, F. J.; Abruña, H. D. Cobalt-Based Nitride-Core Oxide-Shell Oxygen Reduction Electrocatalysts. *J. Am. Chem. Soc.* **2019**, *141*, 19241−19245.

(20) Yang, Y.; Zeng, R.; Xiong, Y.; DiSalvo, F. J.; Abruña, H. D. Rock-Salt-Type $MnCo_2O_3$/C as Efficient Oxygen Reduction Electrocatalysts for Alkaline Fuel Cells. *Chem. Mater.* **2019**, *31*, 9331−9337.

(21) Wei, C.; Feng, Z.; Scherer, G.; Barber, J.; Shao-Horn, Y.; Xu, Z. Cations in Octahedral Sites: A Descriptor for Oxygen Electrocatalysis on Transition-Metal Spinels. *Adv. Mater.* **2017**, *29*, 1606800.

(22) Indra, A.; Menezes, P.; Sahraie, N.; Bergmann, A.; Das, C.; Tallarida, M.; Schmeißer, D.; Strasser, P.; Driess, M. Unification of Catalytic Water Oxidation and Oxygen Reduction Reactions: Amorphous Beat Crystalline Cobalt Iron Oxides. *J. Am. Chem. Soc.* **2014**, *136*, 17530−17536.

(23) Tang, J.; Su, C.; Zhong, Y.; Shao, Z. Oxide-Based Precious Metal-Free Electrocatalysts for Anion Exchange Membrane Fuel Cells: From Material Design to Cell Applications. *J. Mater. Chem. A* **2021**, *9*, 3151−3179.

(24) Yang, Y.; Xiong, Y.; Holtz, M. E.; Feng, X.; Zeng, R.; Chen, G.; DiSalvo, F. J.; Muller, H. D.; Abruña, H. D. Octahedral Spinel Electrocatalysts for Alkaline Fuel Cells. *Proc. Natl. Acad. Sci. U. S. A.* **2019**, *116*, 24425−24432.

(25) Yang, Y.; Peng, H.; Xiong, Y.; Li, Q.; Lu, J.; Xiao, L.; DiSalvo, F.; Zhuang, L.; Abruña, H. High-Loading Composition-Tolerant Co-Mn Spinel Oxides with Performance beyond 1 W/cm^2 in Alkaline Polymer Electrolyte Fuel Cells. *ACS Energy Lett.* **2019**, *4*, 1251−1257.

(26) Yang, Y.; Wang, Y.; Xiong, Y.; Huang, X.; Shen, L.; Huang, R.; Wang, H.; Pastore, J. P.; Yu, S. H.; Xiao, L.; Brock, J. D.; Zhuang, L.; Abruña, H. D. *In Situ* X-Ray Absorption Spectroscopy of a Synergistic Co-Mn Oxide Catalyst for the Oxygen Reduction Reaction. *J. Am. Chem. Soc.* **2019**, *141*, 1463−1466.

(27) Yang, Y.; Xiong, Y.; Zeng, R.; Lu, X.; Krumov, M.; Huang, X.; Xu, W.; Wang, H.; DiSalvo, F. J.; Brock, J. D.; Muller, D. A.; Abruña, H. D. Operando Methods in Electrocatalysis. *ACS Catal.* **2021**, *11*, 1136−1178.

(28) Xiong, Y.; Yang, Y.; Feng, X.; DiSalvo, F. J.; Abruña, H. D. A Strategy for Increasing the Efficiency of the Oxygen Reduction Reaction in Mn-Doped Cobalt Ferrites. *J. Am. Chem. Soc.* **2019**, *141*, 4412−4421.

(29) Clavilier, J.; Faure, R.; Guinet, G.; Durand, R. Preparation of monocrystalline Pt microelectrodes and electrochemical study of the plane surfaces cut in the direction of the {111} and {110} planes. *J. Electroanal. Chem. Interfacial Electrochem.* **1980**, *107*, 205−209.

(30) Yang, Y.; Chen, G.; Zeng, R.; Villarino, A. M.; DiSalvo, F. J.; van Dover, R. B.; Abruna, H. D. Combinatorial Studies of Palladium-Based Oxygen Reduction Electrocatalysts for Alkaline Fuel Cells. *J. Am. Chem. Soc.* **2020**, *142*, 3980−3988.

(31) van Dover, R. B.; Schneemeyer, L. F.; Fleming, R. M. Discovery of a Useful Thin-Film Dielectric Using a Composition-Spread Approach. *Nature* **1998**, *392*, 162−164.

(32) Xiang, X.-D.; Sun, X.; Briceno, G.; Lou, Y.; Wang, K.-A.; Chang, H.; Wallace-Freedman, W. G.; Chen, S.-W.; Schultz, P. G. A Combinatorial Approach to Materials Discovery. *Science* **1995**, *268*, 1738−1740.

(33) Smith, R. D. L.; Prévot, M. S.; Fagan, R. D.; Zhang, Z.; Sedach, P. A.; Siu, M. K. J.; Trudel, S.; Berlinguette, C. P. Photochemical Route for Accessing Amorphous Metal Oxide Materials for Water Oxidation Catalysis. *Science* **2013**, *340*, 60−63.

(34) Reddington, E.; Sapienza, A.; Gurau, B.; Viswanathan, R.; Sarangapani, S.; Smotkin, E. S.; Mallouk, T. E. Combinatorial Electrochemistry: A Highly Parallel, Optical Screening Method for Discovery of Better Electrocatalysts. *Science* **1998**, *280*, 1735−1737.

(35) Eom, C. J.; Kuo, D.-K.; Adamo, C.; Moon, E. J.; May, S. J.; Crumlin, E. J.; Schlom, D. G.; Suntivich, J. Tailoring Manganese Oxide with Atomic Precision to Increase Surface Site Availability for Oxygen Reduction Catalysis. *Nat. Commun.* **2018**, *9*, 4034.

(36) Wakabayashi, R. H.; Paik, H.; Murphy, M. J.; Schlom, D. G.; Brutzam, M.; Uecker, R.; van Dover, R. B.; Disalvo, F. J.; Abruña, H. D. Rotating Disk Electrode Voltammetry of Thin Films of Novel Oxide Materials. *J. Electrochem. Soc.* **2017**, *164*, H1154−H1160.

(37) Ichimiya, A.; Cohen, P. *Reflection High Energy Electron Diffraction*; Cambridge University Press: New York, 2004; p 43.

(38) Bard, A. J.; Faulkner, L. R. *Electrochemical Methods: Fundamentals and Applications*; Wiley: New York, 2001; p 335.

(39) Yang, Y.; Xiao, W.; Feng, X.; Xiong, Y.; Gong, M.; Shen, T.; Lu, Y.; Abruña, H. D.; Wang, D. Golden Palladium Zinc Ordered Intermetallics as Oxygen Reduction Electrocatalysts. *ACS Nano* **2019**, *13*, 5968−5974.

(40) Davis, R. E.; Horvath, G. L.; Tobias, C. W. The Solubility and Diffusion Coefficient of Oxygen in Potassium Hydroxide Solutions. *Electrochim. Acta* **1967**, *12*, 287−297.

(41) Goodenough, J. B.; Manoharan, R.; Paranthaman, M. Surface Protonation and Electrochemical Activity of Oxides in Aqueous Solution. *J. Am. Chem. Soc.* **1990**, *112*, 2076−2082.

(42) Kuo, D.-Y.; Paik, H.; Kloppenburg, J.; Faeth, B.; Shen, K. M.; Hautier, G.; Schlom, D. G.; Suntivich, J. Measurements of Oxygen Electroadsorption Energies and Oxygen Evolution Reaction on $RuO_2(110)$: A Discussion of the Sabatier Principle and Its Role in Electrocatalysis. *J. Am. Chem. Soc.* **2018**, *140*, 17597−17605.

(43) Hu, B.; Kuo, D.-Y.; Paik, H.; Schlom, D. G.; Suntivich, J. Enthalpy and Entropy of Oxygen Electroadsorption on $RuO_2(110)$ in Alkaline Media. *J. Chem. Phys.* **2020**, *152*, 094704.

(44) Rao, R. R.; Kolb, M. J.; Halck, N. B.; Pedersen, A. F.; Mehta, A.; You, H.; Stoerzinger, K. A.; Feng, Z.; Hansen, H. A.; Zhou, H.; Giordano, L.; Rossmeisl, J.; Vegge, T.; Chorkendorff, I.; Stephens, I. E. L.; Shao-Horn, Y. Towards Identifying the Active Sites on RuO_2 (110) in Catalyzing Oxygen Evolution. *Energy Environ. Sci.* **2017**, *10*, 2626−2637.

(45) Kuo, D.-Y.; Kawasaki, J. K.; Nelson, J. N.; Kloppenburg, J.; Hautier, G.; Shen, K. M.; Schlom, D. G.; Suntivich, J. Influence of Surface Adsorption on the Oxygen Evolution Reaction on $IrO_2(110)$. *J. Am. Chem. Soc.* **2017**, *139*, 3473−3479.

(46) Gomez-Marin, A. M.; Rizo, R.; Feliu, J. M. Oxygen Reduction Reaction at Pt Single Crystals: A Critical Review. *Catal. Sci. Technol.* **2014**, *4*, 1685−1698.